Electro-Synthesis of Pure Aqueous H₂O₂ on Nitrogen-Doped Carbon in a Solid Electrolyte Flow Cell without Using Anion Exchange Membrane

^a Chemical and Biological Engineering, Biorenewables Research Laboratory, Iowa State University, Ames, IA 50011, USA

* Correspondence authors.

Wenzhen Li: E-mail: wzli@iastate.edu; Tel: +1-515-294-4582

Keywords: Hydrogen peroxide, On-site generation, Two-electron oxygen reduction, Solid electrolyte flow cell, Metal-free, Nitrogen doping, Electrocatalysis

ABSTRACT

The two-electron oxygen reduction reaction (2e-ORR) generates on-site hydrogen peroxide (H₂O₂) more sustainably than the industrial anthraquinone process. Pure aqueous H₂O₂ electrosynthesis is the most desirable approach, as it is ready-to-use and pH-adjustable. Recently an innovative dual membrane-based solid-electrolyte flow cell (SE-FC_{AEM/CEM}) was reported, in which the anode and cathode "sandwiched" the cation-exchange-membrane (CEM) and anion-exchange-membrane (AEM), separated by a solid-electrolyte, thus allowing H⁺ and HO₂ ions to recombine to form pure H₂O₂ in deionized (DI)-water stream. One key research needs to effectively deploy this flow cell is to address the stability and engineering difficulties of using an AEM, creating significant drawbacks in cell performance and lifespan. Here, we report a modified SE-FC without involving AEM (SE-FC_{AEM-FREE}) to achieve better performance of H₂O₂ electrosynthesis. To validate SE-FC_{AEM-FREE} for industrial-relevant production rates, we first developed a nitrogen-doped-carbon catalyst (N-C) with varied nitrogen-to-carbon ratios. Among all samples, the catalyst N-C(2:3) contains high carbon and a proper nitrogen precursor that boosted its activity, resulting in excellent half-cell performance with faradaic efficiency (FE) above 90% at different pH-electrolytes. Secondly, we optimized the catalyst microenvironment by applying a PTFE layer. The Layered-PTFE (5wt.%) arrangement suppresses hydrogen evolution reaction (HER) and exhibits a high 2e⁻ ORR activity with high current density of 380 mAcm⁻² (about 6.53 mmol cm⁻²h⁻¹) at 90% FE_{H2O2} without degradation for a 50-hour durability test.

1. Introduction

Hydrogen peroxide (H₂O₂) is a valuable and versatile molecule that has been considered a potential oxidant for green and sustainable chemistry [1]. Multi-step anthraquinone oxidation (AO) is the main industrial route to H₂O₂ production. Despite its massive scale and high-purity production, this technology poses major threats to its long-term sustainability and safety due to high energy consumption, difficult industrial waste management, and non-neglected storage and transportation expenses [2]. Another approach that has been extensively studied is the direct catalytic synthesis of H₂O₂ from H₂ and O₂ employing noble-metal catalysts. However, using an explosive H₂/O₂ mixture that presents legitimate hazards to public safety [3]. Innovative, safe, and sustainable on-site H₂O₂ manufacturing processes are urgently needed. In recent years, the twoelectron oxygen reduction reaction (2e⁻ ORR) method for electrochemically generating H₂O₂ has attracted enormous interest [4]. It offers great advantages, including ambient condition reactions, eco-friendly reacting precursors like oxygen and water, compatibility with renewable energy sources, low overall energy consumption, and high energy conversion efficiencies [5-8]. The complete O₂ reduction to H₂O via four-electron oxygen reduction (4e⁻ ORR) is the major side reaction, which is the favored route for fuel cell applications [9]. Although research has focused extensively on developing highly active electrocatalysts, H₂O₂ is typically generated in aqueous electrolytes in acidic to basic pH ranges, requiring additional separation processes to obtain pure H₂O₂ solutions. Early designs employing deionized (DI) water or a polymer electrolyte membrane (PEM) as the ion-conducting electrolyte for synthesizing pure H₂O₂ solutions have been investigated; however, these designs frequently suffered low reaction rates, product concentrations, or Faradaic efficiencies [10-12].

Recently, a milestone work on pure H₂O₂ electrosynthesis has significantly improved the cell performance by employing a solid-electrolyte flow cell (SE-FC_{AEM/CEM}) with dual membranes

to couple oxygen evolution reaction (OER) at the anode with partial ORR at the cathode [13]. Cation-exchange-membrane (CEM) and anion-exchange-membrane (AEM) were placed between the anode and cathode, with the solid-electrolyte in the middle, thus allowing protons (H⁺) and perhydroxyl anions (HO₂⁻) to recombine in the stream of DI water to produce pure H₂O₂. The great advantage of this system is that no post-treatment purification is required, thus making it highly promising for scaling up production. This innovative cell configuration has shaped future strategies of utilizing electrochemical cells for high-performance on-site generation establishing a new benchmark performance, with 200 mAcm⁻² and FE of 84%, for practical flow cell H₂O₂ generation.

While efficient H₂O₂ electrosynthesis catalysts in acidic and alkaline media have been extensively studied, their performances in neutral media have received far less attention, making the development of an electrocatalyst capable of operating such a cell at industrially relevant current densities (hundreds of mAcm⁻²) while maintaining high faradaic efficiency (FE) one of the key challenges in these processes [4, 8, 14-16]. As the cost and rarity of noble metal components make future large-scale deployments challenging, carbon-based materials with surface functionalization, particularly oxygen functional groups, have been reported as one of a few promising low-cost 2e⁻ ORR catalysts in neutral pH [13]. While oxidized carbon (O-C) catalysts have exhibited great H₂O₂ selectivity of over 90%, they typically require large overpotentials to deliver industrial-relevant currents due to their slow kinetics, especially under large currents. This may originate from the high charge transfer resistivity at the catalyst surface caused by surface oxidation [17-19]. On the other hand, untreated carbon catalysts showed limited H₂O₂ selectivity and activity. For future development of H₂O₂ electrosynthesis technology, it is essential to explore

carbon-based catalysts with remarkably high 2e⁻ ORR activity and selectivity at industrially relevant current densities.

Another issue concerning the (SC-FC_{AEM/CEM}) configuration is that the dual membrane design (AEM/CEM) increases the cell voltage due to higher internal resistance, particularly the AEM, has suffered chemical, electrochemical, and mechanical instability issues, especially under the attack from 'OH radicals during the formation of HO₂⁻ anion. Moreover, device integration frequently fails due to engineering difficulties, such as moisture management and AEM-electrode three-phase interface, which inhibit the device from achieving the desired lifetime [20-22]. Hence, achieving superior performance demands exploring alternative solutions to address these AEM shortcomings.

Herein, we reported a modified nitrogen-doped-carbon (N-C) for H₂O₂ electrosynthesis in neutral media following our recent work in the synthesis method for N-doped-carbon [4]. The nitrogen-to-carbon mixing ratio was optimized at 3:2, and electrochemical measurements of 2e⁻ ORR activity in both batch and flow cells at varied pH electrolytes were conducted. In addition, functionalized carbon (O-C) was synthesized and used as a control sample along with an untreated carbon for 2e⁻ ORR activity comparison. Following catalyst optimization, we introduced our modified cell, SE-FC_{AEM-FREE}, to maximize cell performance and overcome barriers caused by involving of AEM. We compared the 2e⁻ ORR activity in the (standard) and (AEM-FREE) SE-FC setups, demonstrating that the latter can surpass the capped activity of the standard design. We also modulated the catalyst microenvironment by applying an additional PTFE layer, which further increased the activity and selectivity of the 2e⁻ ORR, while also enhancing the cathode hydrophobicity and providing an extra layer to protect the catalyst layer. Four configurations were tested, and the optimal configuration (continuous layered PTFE) was obtained to achieve the

maximum partial ORR activity and H₂O₂ production rate, and the 50-hour durability was also evaluated.

2. Materials and methods

2.1 Electrocatalyst preparation

2.1.1 Nitrogen-doped-carbon (N-C) synthesis

The N-C catalysts were synthesized at four nitrogen-to-carbon ratios: (1:4, 2:3,3:2 and 4:1). For N-C(1:4), 0.25 g of glycine (Sigma-Aldrich) was first thoroughly ground with 0.750 g of Ketjenblack carbon or EC-600JD, (AkzoNobel) in an agate mortar. The dry mixture was then transferred to a tube furnace. The powders were initially heated to 500 °C in Argon (Ar) gas at a ramp rate of 3 °C min⁻¹ for 2 h. The temperature was then increased to 800 °C at a ramp rate of 3 °C min⁻¹ for an additional 2 h. The resulting product was used without further treatment. The same approach was used to synthesize N-C(2:3), N-C(3:2), and N-C(4:1) catalysts.

2.1.2 Functionalized carbon (O-C) synthesis.

Briefly, 0.5 g of untreated C was transferred to an oven to be treated at 550 °C for 2 h at a ramp rate of 5 °C min⁻¹. The product was collected without further treatment.

2.2 Material characterization

Materials morphologies were investigated by FEI Quanta 250 field-emission scanning electron microscope (SEM) with an Oxford Instruments AztecTM energy-dispersive spectrometer (EDS). For cross-section analysis, PTFE/carbon-based samples with different configurations were embedded in epoxy and allowed to cure overnight before being polished with sandpapers and diamond suspensions for characterization. Static contact angles were evaluated by a contact anglemeter (MCA-4, Kyowa Interface Science Co., Ltd). Each sample was placed on a flat electrode surface, and one drop of 6 μL DI water was applied to each surface region. The images

were captured within 30 seconds. Each sample was measured in five distinct regions, and the average was estimated. The surface compositions and their corresponding multiple binding energy peaks were investigated by X-ray photoelectron spectroscopy (XPS) with Mg K α alpha X-ray (1253.6 eV) (Kratos Amicus/ESCA 3400). Powder X-ray diffraction (XRD) patterns were acquired from a Rigaku Ultima IV X-ray diffraction XRD system with Cu Ka radiation (λ =1.54056 Å), and scan angle range from 15° to 90°.

Ion chromatography (IC, Thermo Scientific Dionex Easion) was used to investigate the product's purity, specifically to detect alien ions. A 50 or 100 μL sample solution was diluted with deionized water, filtered (2 μm PTFE), and injected into IC for analysis. A calibration curve was constructed for each ion to estimate its concentration.

2.3 Electrocatalytic characterization.

2.3.1 H-shape cell (H-cell) configuration half-cell measurements

The electrochemical measurements were performed in a customized H-shape cell (H-cell) connected to a multi-channel potentiostat (Biologic VSP-300). The H-cell was divided into two compartments by an ion-exchange membrane (Nafion 212). A working electrode and a silver/silver chloride (Ag/AgCl, 3.5M KCl) reference electrode were in one compartment, while platinum foil was in the other compartment (as the counter electrode). Both compartments were filled with either acidic (0.1 M H₂SO₄), neutral (0.1 M Na₂SO₄), or basic (0.1 M KOH) solutions. The cathode was supplied with 25 mL min⁻¹ of O₂ while the electrolyte was stirred at 250 rpm. For K⁺ conducting membrane, it was pretreated for 1 h with 1 M H₂O₂ and then with 1 M KOH at a temperature of 80 °C. The catalyst ink employed in the fabrication of the working electrode was a mixture of dispersed catalyst powder, isopropanol, and a 5% AS-4 (Tokuyama) solution. A catalyst loading of approximately 0.1 mg cm⁻² was sprayed onto carbon paper, Sigracet 22 BB (Fuel Cell Store),

with a square area of 1 cm². All electrode potentials were converted to RHE unless specified otherwise. Prior to electrochemical tests, the electrolyte resistance was corrected using the manual IR compensation (MIR) method. Error bars were included, and all reported results were based on a minimum of three independent trials.

2.3.2 Three-electrode-flow-cell -configuration (3E-FC) half-cell measurements

Electrochemical measurements were carried out in our three-electrode flow cell with a PTFE spacer with an thickness of 8mm. The anode chamber, separated from the cathode by a (Nafion 115) membrane, was pumped with and acidic (1 M H₂SO₄), neutral (1 M Na₂SO₄), or (1 M KOH) solution at 35 mL min⁻¹. A platinized titanium fiber felt catalyst (2 x 2 cm², Fuel Cell Store) was employed on the anode side. In the cathode chamber, one of three electrolyte solutions was cycled at 35 mL min⁻¹ through a custom-made PTFE spacer facing the catalyst and including the reference electrode (Ag/AgCl). The oxygen gas was constantly fed through the back of the catalytic substrate at a rate of 30 mL min⁻¹. The N-C(2:3) catalyst ink was airbrushed on a carbon paper, Sigracet 22 BB (Fuel Cell Store), with an area of 4 cm² (2 cm × 2 cm), resulting in a mass loading of 0.5 mg cm⁻². IR compensation was used in all flow cell measurements. All electrode potentials were converted to RHE unless stated otherwise.

2.3.3 Two-electrode-solid-electrolyte-cell configuration (SE-FC) measurements

a) Standard two-electrode-solid-electrolyte-cell -configuration (SE-FCAEM/CEM)

For the standard two-electrode-solid-electrolyte-cell configuration (SE-FC_{AEM/CEM}), an anion exchange membrane (Sustainion X37-50 Grade RT, Dioxide Materials) and a Nafion 115 (Fuel Cell Store) were employed for anion and cation exchange, respectively. For the cathode and anode, we used about 0.5 mg cm⁻² N-C(2:3) loaded on Sigracet 35 BB and Pt-Ir-Black catalyst (Premetek) loaded on Sigracet 39 AA (1.9 x 1.8 cm²). The cathode side was fed with 35 mL min⁻

¹ of humidified O₂ gas. The anode side was cycled with a 1 M H₂SO₄ aqueous solution at a rate of 6 mL min⁻¹. Dowex 50W X8(Sigma) cation conductors were employed as solid ion conductors packed a custom PTFE spacer (1.5 mm thickness). All two-electrode potentials were manually compensated (90%) unless otherwise noted.

b) Modified two-electrode-solid-electrolyte-cell -configuration (SE-FC_{AEM-FREE})

The SE-FC_{AEM/CEM} experimental settings were used for the modified two-electrode-solidelectrolyte-cell -configuration (SE-FC_{AEM-FREE}), with the exceptions, as indicated below.

First, dry O₂ gas was supplied at 35 mL min⁻¹ instead of humidified O₂ gas. Second, in the SE-FC_{AEM-FREE}, AEM was completely removed, in which the cathode catalyst was in direct contact with the ion conductors. For PTFE layer integration, the mixed configuration (Mixed-PTFE(5wt.%)_{N-C(2:3)}) was prepared by pre-mixing about 5wt.% PTFE nanopowder (Nanoshel, 20-50 nm) with the catalyst ink mixture prior to airbrushing on the catalyst substrate. For the layered configurations (Layered-PTFE(5wt.%)_{N-C(2:3)}) and (Layered-PTFE(10wt.%)_{N-C(2:3)}), a mixture of dispersed PTFE, isopropanol, and a 5 wt.% AS-4 (Tokuyama) solution was prepared, and then about (5 or 10) wt.% PTFE was sprayed onto the catalyst surface with (0.5 mg/cm⁻²) loading. The (no-PTFE_{N-C(2:3)}) configuration without spraying PTFE was used as a reference sample.

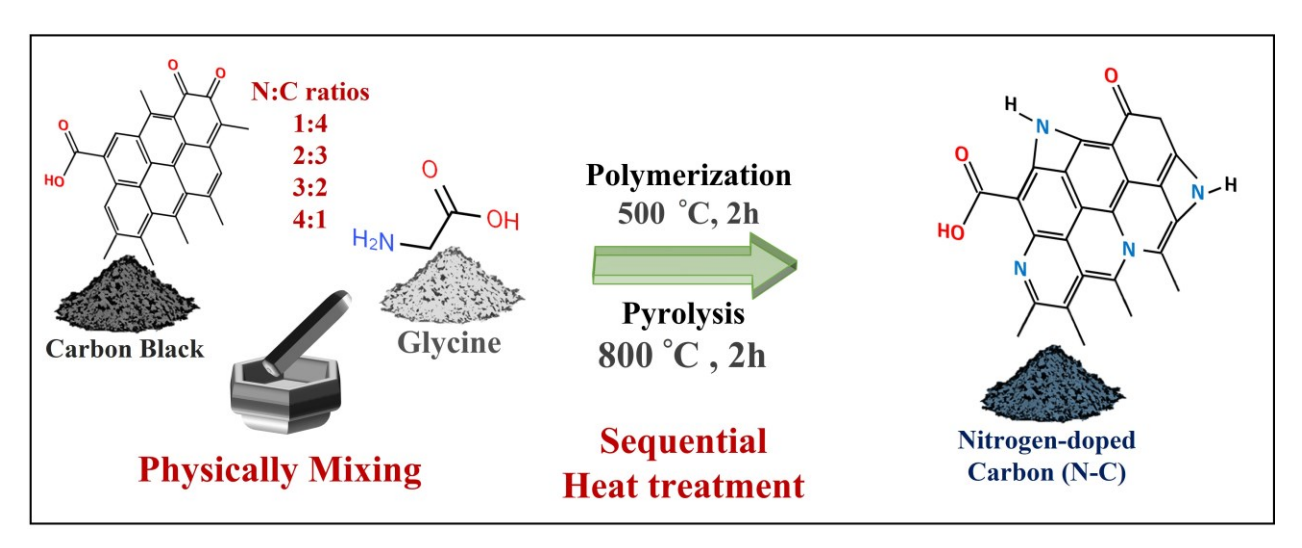
2.3.4 H₂O₂ quantification

The iodide/UV-Vis spectroscopy approach was used to quantify the H₂O₂ produced in each test by collecting samples at certain time intervals. This quantification method has been extensively explained elsewhere [23]. In brief, the collected H₂O₂ sample was mixed to equal amounts of solutions A and B and allowed to combine for 5 minutes. Then, UV-Vis measurements were obtained at 351 nm, and hydrogen peroxide concentrations were measured using a calibration

curve constructed using standard H₂O₂ solution. The Faradaic efficiency of H₂O₂ was calculated by the following equation:

$$H_2O_2$$
 Faradaic efficiency, FE (%) = $\frac{2VCF}{O}$ (1)

Where V is the electrolyte volume (L), volume, C is the H_2O_2 produced concentration (mol L^{-1}), F is the faraday constant (C mol⁻¹), and Q is the total charge passed (C).



Scheme 1. Synthesis procedure of the N-C catalyst with different N:C ratios.

3. Results and discussion

3.1. Catalyst synthesis, 2e⁻ ORR affinity and characterization

3.1.1 Material preparation

Catalysts were synthesized (Scheme 1) by anchoring a nitrogen dopant on carbon support at various nitrogen-to-carbon mixing ratios, and the resulting catalysts were tested for 2e-ORR performance. Ketjenblack carbon (EC-600JD), was selected as the starting material for this study due to its low price, high surface area, and, more importantly, its superior electrical conductivity and morphology, which allows achieving a lower electrical resistance than other commercial carbon blacks, enabling greater conductivity with less carbon amount [24]. Glycine (nitrogen precursor) is an attractive precursor for N-doped carbon synthesis due to its non-toxicity and

widespread availability in large quantities at a reasonable price [25, 26]. For this study, we chose glycine because, upon heating (dehydration), it forms carbon chains with an abundance of N-H bonds, which are believed to be essential for forming pyrrolic-N in the carbon framework [4]. Similar to our earlier work [4], the N-C was synthesized by grinding glycine with carbon at four nitrogen-to-carbon ratios: (1:4, 2:3, 3:2 and 4:1), followed by polymerization (glycine dehydration) and carbonization steps in Ar atmosphere. Our control samples included both untreated carbon and state-of-the-art functionalized carbon (O-C); the latter was synthesized by heating carbon powder in air at 550 °C for 2 hours. Detailed synthesis is provided in Materials and Methods.

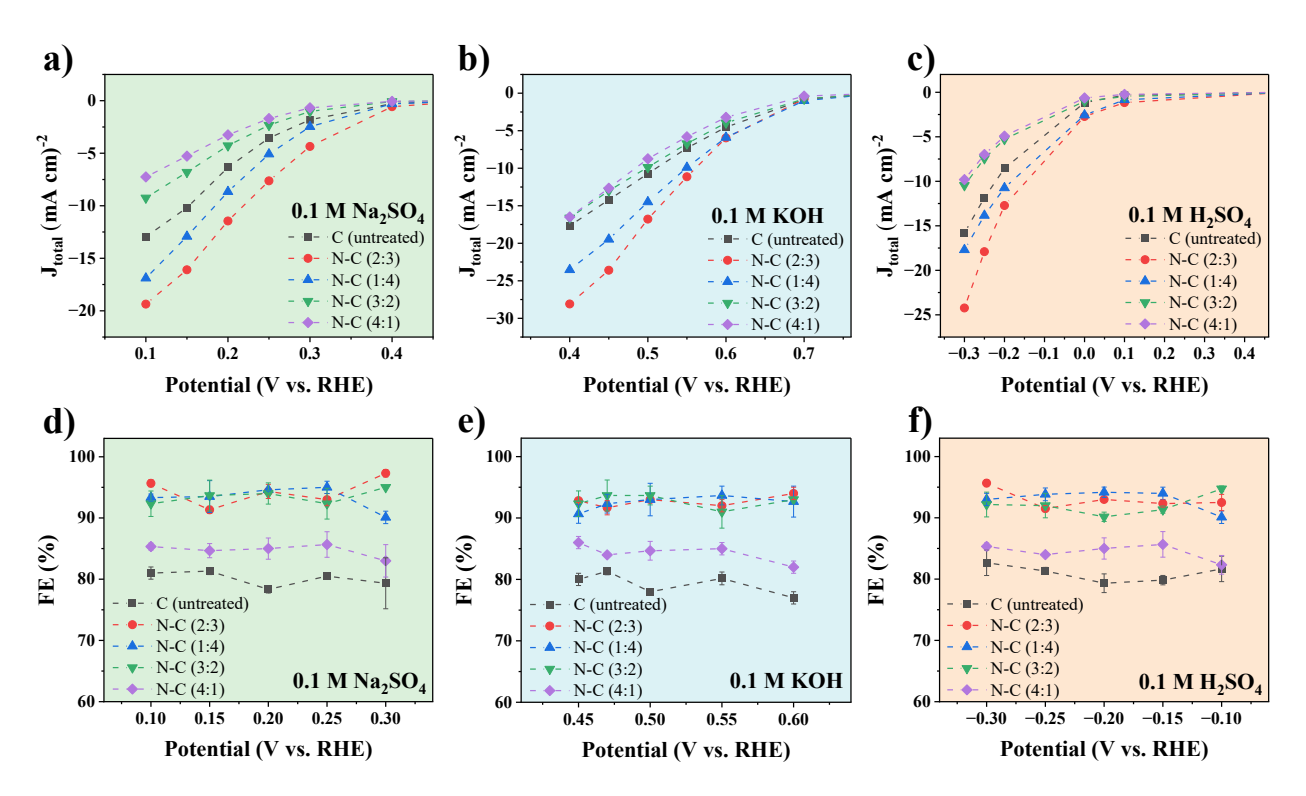


Fig. 1. (a-c) J-E curves and (d-f) the corresponded FE for all N-C catalysts in H-cell at 0.1 M Na₂SO₄, 0.1 M KOH and 0.1 M H₂SO₄ solutions, respectively.

3.1.2 N-C catalysts 2e⁻ ORR affinity

To evaluate their intrinsic 2e⁻ ORR performance, the four N-doped carbon catalysts, as well as untreated carbon, were tested in an H-type electrolysis cell in neutral (0.1M Na₂SO₄), alkaline (0.1M KOH) and acidic (0.1 M H₂SO₄), solutions. Eq. (S1) and (S2) illustrate the standard potential

(E vs. SHE) of the two-electron and four-electron paths in each media. Note that we did not evaluate the molar selectivity using a standard Rotating Ring-Disc Electrode (RRDE) configuration. The H₂O₂ selectivity was reported by FE in our work. This method gives a more exact means of estimating the contribution of ORR activity via the two-electron process at high currents, particularly in the presence of other competing reactions besides those involving H₂O₂ and H₂O. The advantage of using FE as opposed to molar selectivity (obtained from RRDE) has been researched extensively elsewhere [27]. Each catalyst was airbrushed onto a 1 cm² carbon substrate at a loading of 0.1 mg cm⁻². The three electrolyte solutions were oxygen-saturated and stirred at 250 rpm. Fig. 1a–c shows the ORR polarization curves of catalysts with varying nitrogen precursor (glycine) to carbon mixing ratios in an H-cell containing 0.1M Na₂SO₄, 0.1M KOH or 0.1 M H₂SO₄, respectively. The corresponding FE at different potential vs. RHE were plotted in Fig. 1d-f. The incorporation of nitrogen dopants at varying glycine-to-carbon ratios greatly changed the H₂O₂ selectivity relative to the untreated sample. However, in terms of catalytic activity, i.e., current density, N-doped carbon with a lower mixing ratio, as for N-C(1:4) and N-C(2:3) catalyst, exhibited better current density than the baseline sample, while N-Cs with higher mixing ratios performed poorly. Among the four catalysts, N-C(2:3) demonstrated the highest activity, with a current density of 19.4 mA cm⁻² at 0.1 V vs. RHE and a high FE of over 95% across a wide potential window in 0.1M Na₂SO₄. When the mixing ratio was switched to (1:4), (3:2), (4:1), and pure-C, the catalytic activity dropped to 16.9, 9.3, 7.3, and 13 mA cm⁻², respectively. Furthermore, N-C(1:4) and N-C(3:2) showed comparable FE to N-C(2:3), around 92%, whereas N-C(4:1) (FE ~ 85%) increased by only 4% compared to untreated carbon. A similar trend was also observed in both alkaline (Fig. 1b and 1e) and acidic (Fig. 1c and 1f) electrolytes, with N-C(2:3) showing the best activity and selectivity towards 2e ORR. This trend in the H-cell suggests

that the N-C(2:3) sample is the best candidate among various N-doped carbons with different mixing ratios for delivering remarkable ORR density currents while maintaining high H₂O₂ selectivity.

3.1.3 Characterization

The change in morphology could impact catalytic activity. The samples' surface morphology was analyzed using scanning electron microscopy (SEM) to determine whether different mixing ratios can cause morphological changes in the carbon supports. Based on the SEM images shown in Fig. 2a, and Supplemental Fig. S1a, none of the N-doped samples (1:4, 2:3, 3:2, and 4:1 N-C) exhibited apparent differences from the pure-C support of highly dense carbon aggregates. Fig. 2b show the X-ray diffraction (XRD) patterns of all samples. Their XRD peaks were comparable to the pristine sample, with two notable wide, amorphous carbon diffraction peaks centered at 24° and 43° [28]. This result indicated no major structural change during the doping procedure, which is consistent with the observed SEM image. Results from SEM and XRD ruled out morphological influences on the observed performance variation of 2e - ORR in an H-type electrolysis cell.

The successful doping of N into the carbon framework was confirmed by X-ray photoelectron spectroscopy (XPS). Fig. 2c shows wide-scan XPS survey spectra of all N-C samples with peaks corresponding to C_{1s} (285.5 eV), N_{1s} (398.5 eV), and O_{1s} (532.3 eV). We conducted a narrow scan XPS of N_{1s} on all N-C samples to determine the source of the improved H₂O₂ synthesis performance. Fig. 2d reveals the development of pyrrolic-N (398.98 eV) in addition to graphitic-N (400.48 eV), pyridinic-N (397.42 eV), and oxidized-N. (402.08 eV). The peak model employed in this analysis was adapted from an earlier study[29].

Fig. 2e and Table S1 illustrate the atomic percentages of N species in all N-C catalysts, as pyrrolic-N and graphitic-N are the most dominant N species in the carbon framework. We



H₂O₂ generation rate [28, 30]. On the other hand, Pyrrolic N increases the adsorption rate of *OOH intermediate (before dissociating to H₂O₂) and inhibits its further dissociation into *O and *OH intermediates (favoring H₂O formation) [29]. Furthermore, it could alter the catalyst's electrical property, providing additional active sites to promote H₂O₂ generation [16].

Maintaining a pyrrolic N to graphitic-N ratio (P/G) of 1 or above is essential to boost N-Cs selectivity to H₂O₂ [4]. The low FE of the N-C(4:1) sample towards 2e⁻ ORR is attributed to its high graphitic-N content (P/G ratio below 1). Although graphitic-N enhances catalytic activity, it has been reported that a graphitic-N-rich catalyst promotes 4e⁻ ORR [31, 32].

In addition to tuning N species on the carbon framework, the glycine-to-carbon ratio also has a critical influence on the catalytic activity. This is because glycine, the N precursor, is not electrochemically conductive compared to the highly conductive carbon black. Adding more glycine causes a loss in electrocatalytic activity. Therefore, a highly active and selective N-C catalyst needs a higher carbon content and a proper nitrogen precursor amount to fully utilize both precursors. Among all N-C samples, N-C(2:3) was found to possess the optimal ratio that significantly enhanced the ORR activity and H₂O₂ selectivity.

In recent studies, surface oxygen functional groups have shown unique capability to increase H₂O₂ selectivity and activity on various carbon materials [33]. At first, we analyzed our samples' oxygen sources to rule out their impacts in 2e⁻ ORR performance. Although the materials were synthesized in an inert gas (Ar) to avoid the formation of oxygen functional groups, XPS quantitative analysis revealed that all samples, including the pristine carbon (2.4 at.%), contained various oxygen levels. We even treated the pristine carbon sample in a gas mixture (5% H₂ in Ar) to maximally remove O₂, but it still retained about 3 at.%. It is worth mentioning that glycine, the nitrogen precursor, may release a trace amount of oxygen during the polymerization step, leading

to the formation of carbon-oxygen bonds. However, it has been demonstrated that the formed nitrogen species, rather than the traced oxygen, is essential in the 2e ORR process [30]. We assume that the surface oxygen primarily resulted from the adsorption of water species and oxygen in the air during the preparation and transfer of these samples, with possible remaining oxygen that could not be eliminated after annealing at 800 °C. Our tests revealed that the traceable surface oxygen present in undoped samples had no affinity for promoting ORR activity since its FE was less than that of the optimized N-C samples. We also intentionally synthesized oxygen-functionalized carbon (O-C) with ~ 11.5 at.% O₂ via heat treatment in air at 550 °C to investigate if the O functional group can promote 2e- ORR. The O-C was more active than the untreated sample, as demonstrated in the following section.

The presence of trace metals, which may affect the oxygen reduction reaction to either H₂O or H₂O₂, pathways was also explored. To rule out the presence of metals, we analyzed the bulk composition of our optimal sample, N-C(2:3), using cross-sectional SEM/EDS (Fig. S3a-b and Table S2) at three distinct locations: substrate, catalyst, and PTFE layer. The bulk analysis revealed that none of the sample's layers contained any trace of metal. In addition, the XPS surface analysis presented in Table S3 verified the presence of only C, N, and O, with no metal peaks near the sample's surface. Accordingly, the bulk and surface chemical composition analysis suggested that our N-doped carbon catalysts are metal-free.

3.2. Electrocatalytic analysis

3.2.1 Electrocatalytic 2e⁻ ORR performance of N-C(2:3)

Based on the cathodic half-cell testing of 2e⁻ ORR performance, we concluded that, of all N-C catalysts with different nitrogen-to-carbon mixing ratios, N-C(2:3) is the optimal mixing ratio for generating significant ORR currents while maintaining high H₂O₂ selectivity. To support our hypothesis, we compared its 2e⁻ ORR performance with two control samples: oxidized-C (O-C)

and pristine-C. A neutral electrolyte (0.1 M Na₂SO₄) was selected since its pH was hypothesized to be similar to the local pH of the DI water/solid conductor configuration where pure aqueous H₂O₂ is produced. Briefly, several factors involving the H⁺ crossover from the anode, solid conductor acidity, and deionized catholyte could alert the microenvironment close to the catalyst surface, resulting in a shift in the local pH ranging from mildly acidic to neutral. Moreover, the indirect estimation (as shown in Fig. S4) of the local pH by comparing the measured 2e⁻ORR onset potentials in three different pH solutions: 0.298 V-RHE in 1 M Na₂SO₄ (neutral), 0.258 V-RHE in DI water (with solid conductors), and 0.732 V-RHE in 1 M KOH (alkaline), showing that ORR is more kinetically favorable in the alkaline electrolyte than that in neutral and acidic electrolytes, which is consistent with previous study [34, 35]. The onset potential data also support our hypothesis that 2e⁻ORR occurred in mildly acidic to neutral but far from alkaline in the DI water/solid conductor arrangement.

The Faradaic efficiency vs. potential (FE–E) curves of different catalysts were plotted in Fig. 3a. Pristine-C showed the lowest FE (~ 79% in a wide potential range) compared to the other two samples, suggesting that the pure carbon without doping did not significantly promote H₂O₂ generation. In contrast, at the same potential range, both N-C(2:3) and O-C catalysts exhibited high H₂O₂ selectivity with FE of >90%. To acquire deeper understanding of their enhanced H₂O₂ activity and kinetic behaviors, Tafel plots were used, as shown in Fig. 3b. The N-C(2:3) sample exhibited the best Tafel slope under neutral conditions, with a value of 78 mV dec⁻¹, which is less than O-C (92 mV dec⁻¹) and Pristine-C (110 mV dec⁻¹). Additionally, double-layer capacitance (C_{dl}) was also measured to compare the ECSA (Fig. 3c inset plot). The calculated C_{dl} was 2.9, 2.6, and 2.5 mF cm⁻² for N-C(2:3), O-C, and pristine-C, respectively, indicating that N-C(2:3) can provide slightly more electrocatalytic active sites for 2e⁻ ORR. We further compared the ECSA-

normalized H₂O₂ current density over the three catalysts (Fig. 3c). The untreated carbon exhibited the most sluggish 2e⁻ ORR activity compared to the other two samples, indicating that further treatments are required to boost its performance. Although the O–C catalyst exhibits a marginally positive onset potential, its catalytic performance was immediately surpassed by N-C(2:3) at high current densities (>5mA cm²).

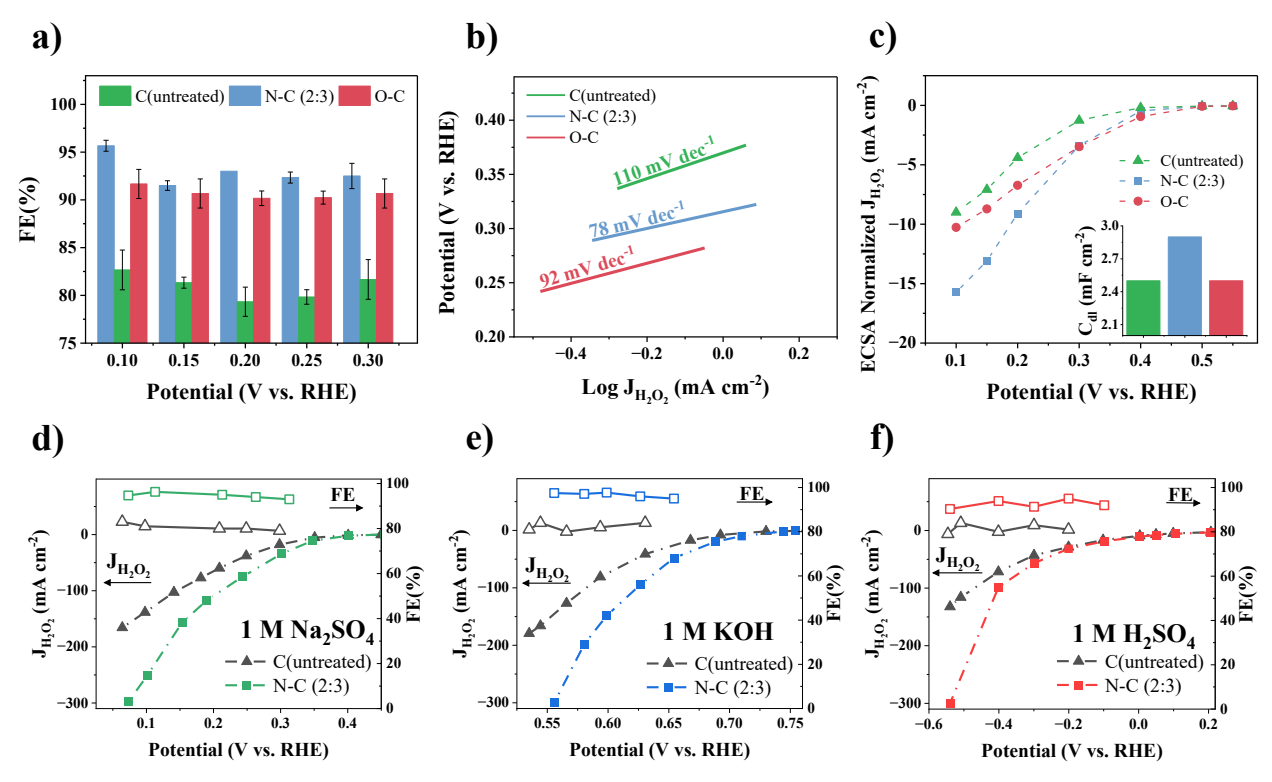


Fig. 3. (a) FE-E plots. (b) Tafel plots. (c) ECSA normalized partial H_2O_2 current density, (inset) double-layer capacitance (C_{dl}) of pristine-C,N-C(2:3) and O-C in H-cell in 0.1 M Na₂SO₄. (d-f) $J_{H_2O_2}$ -E (left) and FE-E(right) plots of pristine-C and N-C(2:3) in 3E-FC in 1M NA₂SO₄, 1M KOH and 1M H₂SO₄, respectively.

The activity of N-C(2:3) was enhanced even further at higher current densities. For instance, in delivering 10 mA cm², N-C(2:3) showed around 100 mV lower overpotential compared to O-C, indicating its significantly faster reaction kinetics. At 0.1 V vs. RHE, the H₂O₂ partial current of N-C(2:3) increased approximately 1.5-fold over O-C. Hence, these results suggested that N-

C(2:3) is the optimal candidate, as its relatively high intrinsic activity maximized its overall 2e⁻ ORR performance.

3.2.2 Three-electrodes flow cell 2e⁻ ORR performance of N-C(2:3)

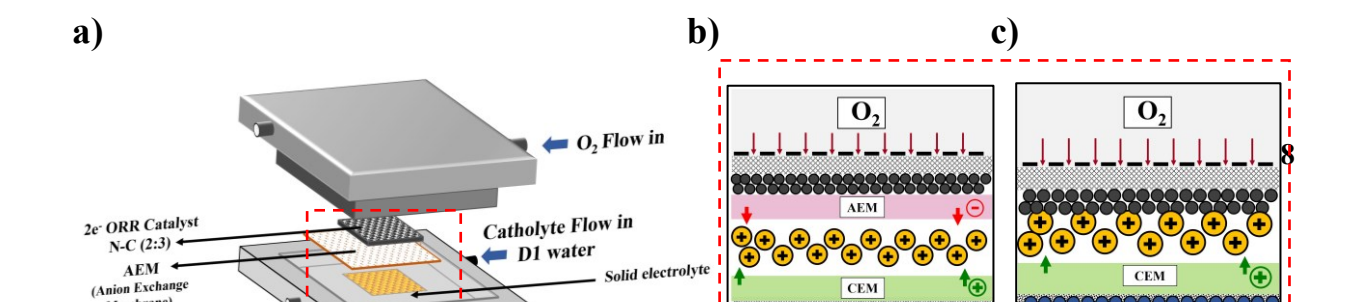
In half-cell 2e⁻ ORR performance, the N-C(2:3) catalyst exhibited facile kinetics, making it a highly promising candidate for delivering industrial-relevant current without sacrificing excellent H₂O₂ formation efficiency. To validate its practical performance, a three-electrodes flow was employed to examine the 2e⁻ ORR performance. It is worth noting that the flow cell configuration is ideal for upscale synthesis because it can improve oxygen gas diffusion to obtain larger ORR current densities while providing more uniform and better mass transport than that in an H-type cell [36]. Fig. S7a-b shows our custom-built three-electrode flow cell (3E-FC) that was utilized to evaluate the 2e⁻ ORR performance of the N-C(2:3) catalyst. The oxygen gas was fed to the back of the catalytic substrate, while the neutral (1M Na₂SO₄), alkaline (1M KOH), and acidic (1M H₂SO₄) electrolytes were cycled in a spacer facing the catalyst layer. Additional information on the cell is provided in the experimental section. Fig. 3d shows the partial current density vs. potential $(J_{H_2O_2}$ -E) and (FE-E) curves of N-C(2:3) and the reference sample, pristine-C, in neutral media. In contrast to the modest 2e⁻ ORR activity and selectivity on pristine-C throughout the potential range, N-C(2:3) achieved remarkable $J_{H_2O_2}$ of 300 mA cm⁻², while maintaining FE of >94%, suggesting outstanding ability to H₂O₂ generation in neutral media. At currents of >30 mA cm⁻², the difference in H₂O₂ activity between the two catalysts was more pronounced. In addition, N-C(2:3) showed facile kinetics in a large current region, with a 90 mV lower overpotential than the reference sample at 150 mA cm⁻². At a constant applied potential of 0.1 V vs. RHE, the H₂O₂ partial current of N-C(2:3) was 1.8 times greater than that of pure-C. Similar trends were seen when the electrolyte was switched to alkaline (1M KOH) and acidic (1M H₂SO₄) solutions, as shown in Fig. 3e-f. N-C(2:3) maintained FE of >93% at the whole potential range in both

electrolytes. Moreover, the H₂O₂ partial current of N-C(2:3) was nearly double that of pure-C at constant applied potentials of 0.55 V vs. RHE (1M KOH) and -0.53 V vs. RHE (1M H₂SO₄), confirming its superior intrinsic activity in all media.

3.2.3 Pure Aqueous H₂O₂ Electrosynthesis

3.2.3.1 Solid Electrolyte flow cell configuration, SE-FCAEM/CEM

With the exceptional 2e⁻ ORR performance that N-C(2:3) demonstrated in the 3E flow cell configuration, we examined its 2-electrode cell (full-cell) performance by coupling it with oxygen evolution reaction (OER) at the anode. We used a solid electrolyte flow cell (SE-FC) configuration to electrosynthesize pure aqueous H₂O₂ ready for immediate use as opposed to a salt-based liquid electrolyte, which would have required post-separation, hindering the cell's scale-up applications. SE-FC also has advantages as it can offer no ion impurity as HO₂⁻ and H⁺ are combined to form H₂O₂, high ion conduction, and low ohmic loss. Fig. 4a-b shows the configuration of the SE-FCAEM/CEM unit that enables direct electrosynthesis of pure H₂O₂ solutions. This cell paired OER at the anode with 2e⁻ ORR at the cathode. Streams of 1 M H₂SO₄ and humidified O₂ (to increase AEM lifespan) were supplied to the anode and cathode catalysts, respectively, in which both catalysts covered gas diffusion layer (GDL) electrodes. The N-C(2:3) catalyst or untreated carbon (baseline) was used in the cathode coupled with Pt-Ir/C, the OER catalyst in the anode. The anode and cathode "sandwiched" the AEM and CEM layers to minimize flooding by liquid water. In the middle, a thin and porous solid electrolyte layer permitted ionic recombination of H⁺ and HO₂⁻ ions crossing from the anode and cathode with minor ohmic losses; a flowing DI water stream confined to this central part (spacer) could then dissolve the pure H₂O₂ in a weak acidity solution of pH ~6 to 7 without extra ionic contamination.





rate of about 1.3 mmol-H₂O₂ cm⁻² h⁻¹ was three times that of the untreated sample, which exhibited unsatisfactory 2e⁻ ORR performance. While the N-C(2:3) did demonstrate improved performance of pure H₂O₂ generation in the SE-FC_{AEM/CEM} unit, the current density must be increased by a few hundred to reach industrially relevant current level. Given that the catalyst layer and ion exchange membrane are the crucial components of a flow cell to reach maximum performance, more optimizations are required to improve their performance. In terms of catalysts, our 2e⁻ ORR catalyst, N-C(2:3), and the commercial OER catalyst, Pt-Ir/C, have demonstrated superior half-cell activity at the cathode and anode [37, 38]. However, for ion exchange membranes, it has been noted that AEM can significantly degrade the cell performance caused by their chemical, electrochemical, and mechanical instability issues. In addition, device integration typically fails due to engineering challenges, such as moisture management and AEM-electrode three-phase interface optimization, which prevent the device from achieving the desirable lifespan [22]. Therefore, the demand for higher performance requires exploring alternative strategies to addressing these shortages of using AEMs.

3.2.3.2 Solid Electrolyte flow cell without an anion exchange membrane (AEM), SE-FC_{AEM-FREE}

Maximizing the cell performance is the primary goal of our work, and eliminating AEM is the key strategy. We proposed employing an AEM-free solid electrolyte flow cell (SEF-C_{AEM-FREE}) to mitigate issues associated with use of AEMs. The SE-FC_{AEM-FREE} unit has an identical design to the standard SE-FC unit except for no integrated AEM, as shown in Fig. 4c. The novel cell assembly has advantages over the conventional design, such as dry O₂ being fed instead of humidified O₂ to the back of the cathode, hence avoiding the cost of providing humidified feedstock. In addition, the voltage drop caused by an AEM and its instability issues are no longer present; therefore, achieving high and durable performance is possible. To examine the impact of eliminating AEM, we compared the catalytic activity of N-C(2:3) in an AEM-free SE-FC to that

of a standard SE-FC in Fig. 4f. Upon AEM elimination, N-C(2:3) was able to achieve a current density of 300 mA cm⁻² at a cell potential of 2.4V, a threefold increase compared to the flow cell with an AEM, indicating improved ionic conductivity. However, the H₂O₂ FE decreased significantly to 65% with the AEM-FREE design as compared to the AEM/CEM design (over 90%). This result suggested that other competitive reactions have occurred concurrently with 2e⁻ ORR within the potential window.

To explore this further, we carried out a control experiment in an AEM-FREE 3E-electrode flow cell with Ag/AgCl as a reference electrode and solid conductors packed in the middle compartment. At the cathode, N2 and O2 were alternately purged while the current was collected with varying potentials to study a possible competitive reaction. Under an N2-saturated environment, the current versus potential (I-E) curves in Fig. S8a revealed the hydrogen evolution reaction (HER) indeed occurred in the potential window with an onset potential (Eonset) of -0.2 V vs. RHE. When the gas was switched to O₂, the ORR window can be distinguished with a more positive E_{onset} around (0.3 V vs. RHE). The HER window was also observed in acidic (1M H₂SO₄) and neutral (1M Na₂SO₄) electrolytes with the same cell design (without ion conductors) at E_{Onset} -0.3 V vs. RHE and -0.15 V vs. RHE, respectively, this ruled out the possibility that the collected current was caused by the ion-conductors degradation from close contact with the catalyst layer (Fig. S8b-c). These results also indicated the existence of a potential mixed zone in the SOFCAEM-FREE unit where both ORR and HER could occur. Carbon catalysts may need significant overpotentials even more negative than 0 V vs. RHE to reduce O₂ to H₂O₂ in solutions with a pH of less or close to 7 [27, 39, 40]. Also, in some cases, large polarizations are necessary to achieve industrial-relevant currents [13, 41]. Under such negative potentials, the HER becomes a likely

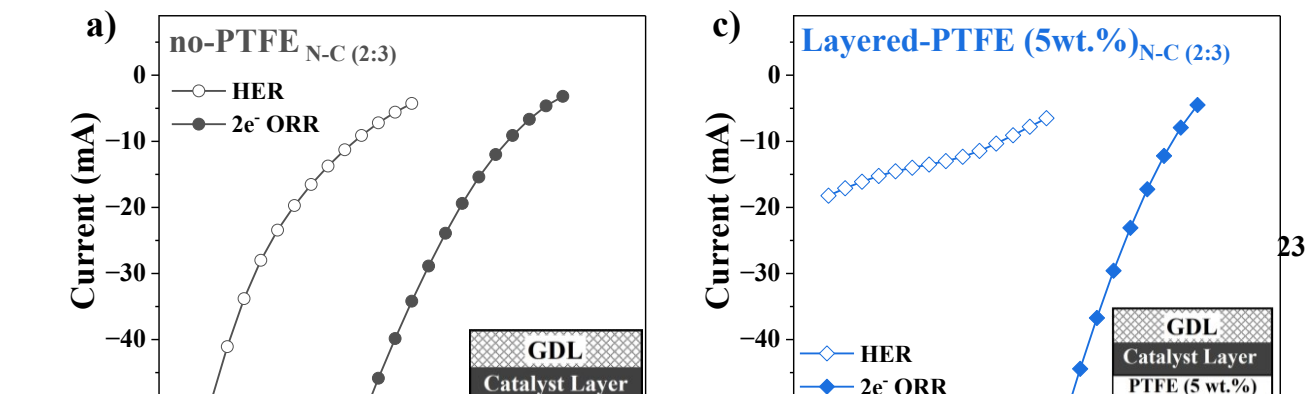
side reaction that must be considered. Thus, to further improve the SOFC_{AEM-FREE} design towards more practical applications, it is necessary to first suppress HER.

3.2.3.3 PTFE layered configuration for HER suppression

Our strategy to suppress HER was to prevent DI water (the H₂O₂ collecting medium) from excessively wetting the catalyst surface, given that in the SE-FC AEM/CEM configuration, in which AEM prevented the catalyst flooding, no ORR/HER mixed region was observed (FE to H₂O₂ 92%) throughout the entire potential window). In the absence of an AEM, like in SOFC AEM-FREE, a extra PTFE layer can sufficiently prevent DI water from excessively soaking the catalyst surface, facilitating O₂ access to the active sites, hence promoting 2e⁻ ORR over HER. We hypothesized that PTFE would suppress HER, but it also has other potential benefits, such as preventing catalyst flooding due to its high hydrophobicity and providing an extra layer of protection for the catalyst layer (e.g. the layered samples were less vulnerable to damage from pressing by the solid ionconducting powders), which is in very close contact with the ion conductors in a flow cell configuration and, thus vulnerable to damage from excessive pressing and crushing by the solid ion-conducting beads. In order to determine the optimal PTFE loading and incorporation techniques for maximizing the benefits of involving the PTFE layer, we compared four alternative configurations shown in Fig. 4g: no-PTFE_{N-C(2:3)}, Mixed-PTFE(5wt.%)_{N-C(2:3)}, Layered-PTFE(5wt.%)_{N-C(2:3)}, and Layered-PTFE(10wt.%)_{N-C(2:3)}. As with the no-PTFE_{N-C(2:3)} configuration, the mixed-PTFE(5wt.%)_{N-C(2:3)} arrangement is constructed by spraying a substrate with a proper amount of N-C(2:3) dispersed in IPA and anion conducting ionomers, AS-4 but with the addition of PTFE (5wt.%) powder to the catalyst ink mixture. For the layered arrangement, the catalyst was sprayed onto the substrate before a continuous PTFE layer (dispersed in IPA and AS-4) of either 5 wt.% or 10 wt.% PTFE was applied, yielding Layered-PTFE(5wt.%)_{N-C(2:3)} and Layered-PTFE(10wt.%)_{N-C(2:3)}. Since PTFE is an inherently non-conductive substance, adding an anion

conducting ionomer within the formed PTFE layer is essential to enable ions to move from or into the catalyst surface. Although this PTFE-ionomer integration is susceptible to losing a portion of its hydrophobicity, the generated OH₂⁻ can freely vacate the catalyst surface to the middle chamber, offering AEM-like characteristics but minimizing chemical and mechanical drawbacks compared to AEM integration. The performance of the four distinct arrangements in an AEM-free 3E-electrode flow cell fed with N₂ and O₂ alternatingly was shown in Fig. 5a-d. Under N₂ saturated environment, in which HER is more pronounced, the catalyst activity to HER was observed from low to high: Layered-PTFE(10wt.%)_{N-C(2:3)} < Layered-PTFE(5wt.%)_{N-C(2:3)} < Mixed-PTFE(5wt.%)_{N-C(2:3)} < no-PTFE_{N-C(2:3)}. Upon O₂ feeding, the 2e⁻ ORR activity from high to low was as follows: Layered-PTFE(5wt.%)_{N-C(2:3)} > no-PTFE_{N-C(2:3)} > Layered-PTFE(10wt.%)_{N-C(2:3)} > Mixed-PTFE(5wt.%)_{N-C(2:3)}.

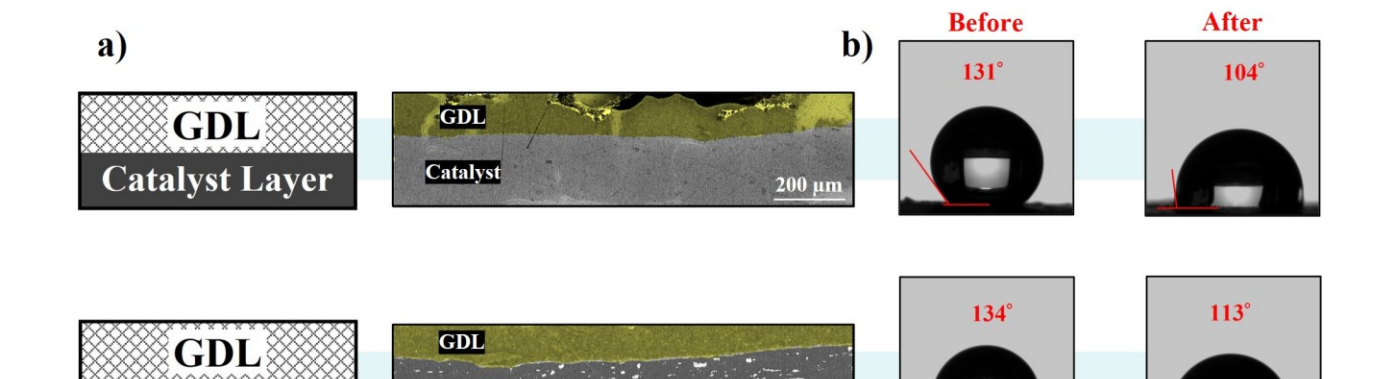
Fig. 5e shows the total current within the mixed HER/2e⁻ ORR region. Among all configurations, Layered-PTFE(5wt.%)_{N-C(2:3)} performed the best, inhibiting HER significantly and exhibiting substantial activity of 2e⁻ ORR. Furthermore, the Layered-PTFE(5wt.%)_{N-C(2:3)} arrangement achieved the highest total mixed current of 185 mA (accounting for 91% of 2e⁻ ORR) at -0.65 V vs. RHE. For the performance of other configurations at the same potential, the total mixed current ranges from 130 mA (69% for 2e⁻ ORR) for no-PTFE_{N-C(2:3)}, 97 mA (93% for 2e⁻ ORR) for Layered-PTFE(10wt.%)_{N-C(2:3)} to 79 mA (77% for 2e⁻ ORR) for Mixed-PTFE(5wt.%)_{N-C(2:3)}.



These results indicate that the addition of PTFE suppressed HER for both (layered) and
(mixed) configurations, but to a greater extent in the former, because a uniform layer of PTFE (1
to 1.5 μ m for PTFE(5wt.%) layer, 10 to 15 μ m for PTFE (10wt.%) layer), as revealed by cross-

sectional SEM images (Fig. 6a), could more effectively block DI water from penetrating the catalyst layers than scattered PTFE spots (mixed). To further study their water-repellent ability, static contact angle measurements were performed on the samples' surface before and after electrochemical testing (Fig 6b). Before testing, all configurations exhibited hydrophobic properties with a contact angle of more than 125° degrees, roughly comparable to the surface measurement of a PTFE-pretreated carbon substrate, 138° degrees (Fig. S9b). However, after one hour of testing involving direct contact with the DI water stream, the contact angle sharply reduced in both no-PTFE_{N-C(2:3)} and Mixed-PTFE(5wt.%)_{N-C(2:3)} to 104° and 113°, respectively, indicating possible DI water wetting issues could occur.

However, the contact angle was marginally decreased to (123°) for Layered-PTFE(5wt.%)_{N-C(2:3)} and (124.5°) for Layered-PTFE(10wt.%)_{N-C(2:3)}, demonstrating that the thin uniform PTFE layer can greatly hinder water wetting the active sites, allowing O₂ to be reduced to OH₂⁻ while simultaneously suppressing HER. Furthermore, the PTFE layer helped to shield the catalyst layer from any possible mechanical stress that might have been applied by the solid conductors (Fig. S10a-d). The top-view SEM image of the samples' surface after testing revealed fewer cracks in the layered configurations than in the mixed configuration, while the no-PTFE configuration exhibited the most damaged surface likely due to solid conductors' close interactions without a protective layer.



3.2.3.4 Performance of modified catalysts with PTFE in SE-FCAEM-FREE
When all four configurations were tested in SE-FCAEM-FREE, their performance was quite
similar to that in 3E-FC, as shown in Fig. 6c. At a cell potential of 1.8V, where 2e ⁻ ORR is

dominant, all four designs displayed excellent FE (over 90%) to H₂O₂. Upon increasing the cell potential, the layered designs (5 wt.% and 10wt.% PTFE) maintained FE of >90%, suggesting that PTFE inhibited HER in the mixed region.

However, both no-PTFE and (mixed) PTFE samples exhibited a significant drop in FE, indicating the presence of two competitive reactions (HER and 2e⁻ ORR) occurred as the cell potential increased (the cathode potential shifted more negatively). Between the two layered arrangements, Layered-PTFE(5wt.%)_{N-C(2:3)} demonstrated the best performance by greatly suppressing HER and being highly active for 2e⁻ ORR as the current density reached 250 mA cm⁻ with FE 90%. Therefore, there was a trade-off between suppressing HER and enhancing ORR. The PTFE amount in Layered-PTFE(5wt.%)_{N-C(2:3)} was the optimal spot for maximum activity. When the PTFE wt.% was increased over 5 wt.%, HER suppression improved, but ORR activity dropped, as seen from the Layered-PTFE(10wt.%)_{N-C(2:3)} design.

3.2.3.5 Pure H₂O₂ generation in SE-FC_{AEM-FREE} over Layered-PTFE(5wt.%)N-C(2:3)

Given that the best performance was obtained by Layered-PTFE(5wt.%)_{N-C(2:3)}, we investigated its performance (Fig. 7a-b) over a wider potential range and found that it was remarkably able to sustain the FE to >90% in the whole potential range (1.7 - 2.35 V) achieving a maximum current density of about 380 mA cm⁻². At a total current of 389 mA cm⁻², or approximately 350 mA cm⁻² of H₂O₂ partial current, a high production rate of 6.53 mmol cm⁻² h⁻¹ was reached. Furthermore, at fixed current density and DI water flow rate of 200 mA/cm⁻² and 0.1 mL min⁻¹, respectively, the H₂O₂ concentration reached 6 wt.% of pure H₂O₂ (Fig. 7c). With a constant current (about 1.2 mmol cm⁻² h⁻¹) of 70 mA cm⁻², the catalyst was stable for at least 50 hours while producing 0.22 mol L⁻¹ H₂O₂ (Fig. 7d). This catalyst was quite stable in the solid electrolyte generation of pure H₂O₂, as the FE maintained around 90% over the whole test range.

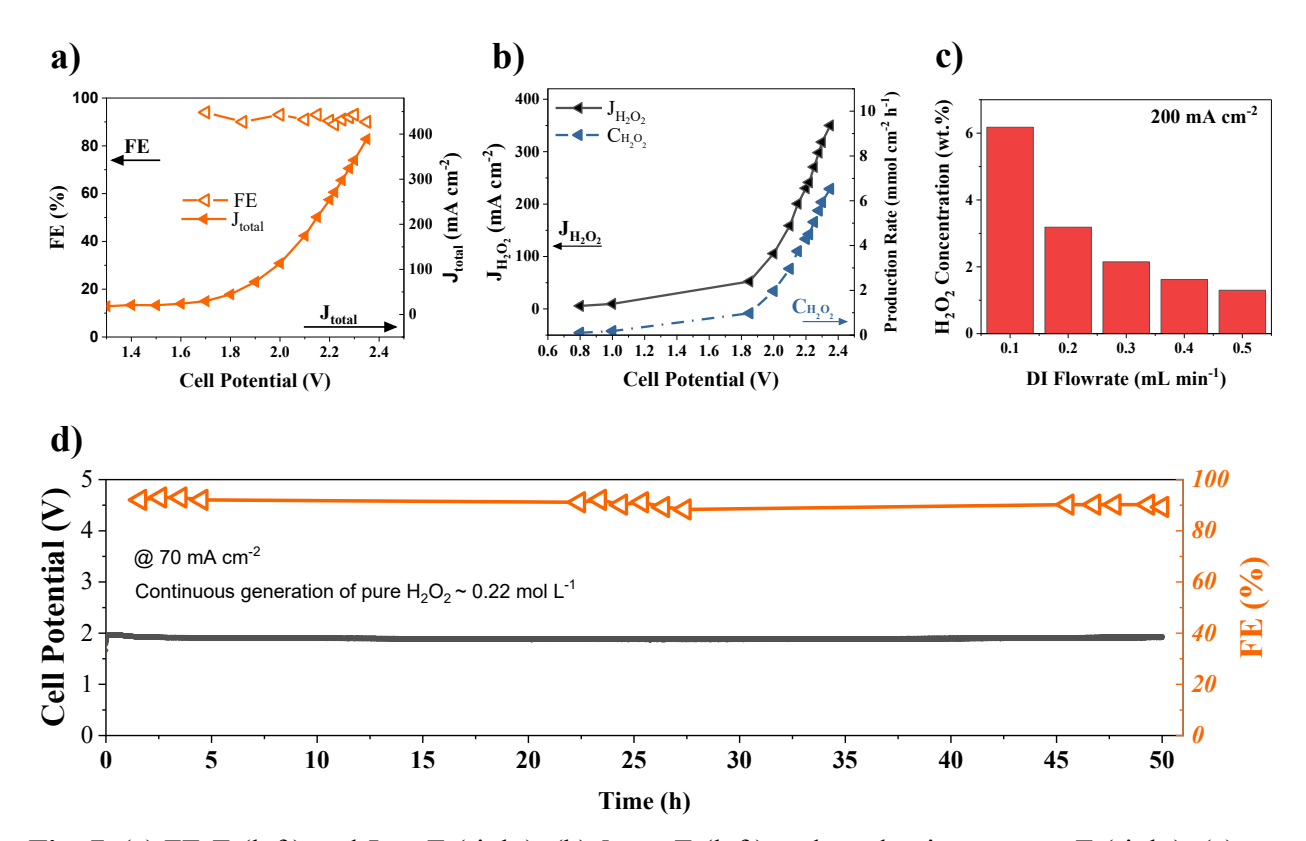


Fig. 7. (a) FE-E (left) and J_{total}-E (right). (b) $J_{H_2O_2}$ -E (left) and production rate vs. E (right). (c) H₂O₂ concentration vs. DI flow rate at 200 mA cm⁻² of Layered-PTFE(5wt.%)_{N-C(2:3)} performance in SE-FC_{AEM-FREE} with . (d) 50 h durability test at 70 mA cm⁻² of Layered-PTFE(5wt.%)_{N-C(2:3)} in SE-FC_{AEM-FREE}. R_{Ω, avg} value of (1.7 Ω) with 90% manual compensation in all above figures.

With a superior Layered-PTFE(5wt.%)_{N-C(2:3)} and further modification of the catalyst microenvironment (PTFE layer), the cell was able to generate hundreds of (mA) of current, validating the use of SE-FC_{AEM-FREE} and demonstrating the superior performance of our Layered-PTFE(5wt.%)_{N-C(2:3)} catalyst in an actual whole-cell. We also validated using dry-O₂ rather than wet-O₂ (Fig. S11). The FE-E plots revealed no apparent change in FE when either dry or wet O₂ was utilized, making the SE-FC_{AEM-FREE} more cost-effective since humidified O₂ is not required.

To evaluate the product's purity, ion chromatography (IC) was used to examine possible ion leaching. Only one intense peak of alien ions corresponding to sulfate ions (SO_4^{2-}) with a level

of (~ 3.7 ppm) was observed in all three independent runs, as shown in Fig. S12 and inset table a. Thus, our AEM-FREE flow cell can generate highly pure H₂O₂ as no significant amounts of foreign ions are present.

Therefore, the enhanced cell and catalyst would provide a promising first step toward the ultimate objective of on-site, industrial-scale electrochemical H₂O₂ generation.

Table S4 summarizes the performances of H₂O₂ bulk production in various flow cells. As compared to the benchmark performance of H₂O₂ synthesis in SE-FC_{AEM/CEM} [13], the cell's peak performance was 200 mAcm⁻² and 84% FE_{H2O2} (about 3.3 mmol cm⁻²h⁻¹) with an energy efficiency (ε_e) of 34.78% at 2.13 V. At a similar E_{cell} (2.15 V), our SE-FC_{AEM-FREE} produced 216 mAcm⁻² and 93% FE_{H2O2} (approximately 3.75 mmol cm⁻²h⁻¹) with ε_e (38.15%).Furthermore, the AEM-FREE cell peak performance exceeded 380 mAcm⁻² while maintaining an exclusive activity of nearly 90 % FE towards H₂O₂ synthesis with at least 50 h durability surpassing the benchmark performance and setting a new standard in this field.

In addition, we conducted preliminary economic analysis of the AEM-FREE cell, as shown in Note 1 in Supporting Information. The operating costs were calculated to be \$ 0.692/kg-H₂O₂, which is lower than the costs of \$0.861/kg-H₂O₂ for currently industrial AQ process without counting storage and transportation costs indicating that our AEM-FREE cell has great potential to compete with the commercial AQ based on its present performance, which could be further improved.

4. Conclusion

We have successfully synthesized nitrogen-doped carbon with an optimal nitrogen-tocarbon mixing ratio (2:3) which showed superior half-cell 2e⁻ ORR activity at various pH electrolytes. The combined characterizations to investigate the catalyst morphology, element

compositions, and N-active species near the surface showed that N-C(2:3) has the optimal properties to exclusively promote H₂O₂ with high activity. This catalyst also outperformed the previously reported O-C as it exhibited facile kinetic with an H₂O₂ partial current increase of about 1.5-fold over O–C at the same potential. With the remarkable 2e⁻ ORR performance that N-C(2:3) exhibited in the 3E flow cell design, we investigated its 2-electrode (full-cell) in a standard SE-FC_{AEM/CEM} as FE maintained >92% throughout the whole potential range. Next, we introduced our modified cell, SE-FCAEM-FREE, to maximize the cell performance aiming to reach hundreds of currents and overcome obstacles caused by AEM integration. Upon optimizing the catalyst microenvironment by applying a PTFE layer, we discovered that the Layered-PTFE(5wt.%)_{N-C(2:3)} configuration exhibited the best performance by significantly suppressing HER and exhibiting high activity for 2e⁻ ORR, with current density reaching 380 mA cm⁻², yielding 6.53 mmol cm⁻² h⁻ ¹ at a FE of 90%. A 50-hour durability test was conducted, and stable performance was demonstrated by maintaining FE above 90%. Our modified SE-FC_{AEM-FREE} with the N-C(2:3) catalyst produced 216 mAcm⁻² and 93% FE_{H2O2} (approximately 3.75 mmol cm⁻²h⁻¹) with ϵ_e (38.15%) at 2.15 V, which surpassed the peak performance of 200 mAcm⁻² and 84% FE_{H2O2} (about 3.3 mmol cm⁻²h⁻¹) of \mathcal{E}_{e} (34.78%) at 2.13 V operation for the previously reported benchmark performance SE-FC_{AEM/CEM}. This work has built a solid foundation for accomplishing the goal of on-site, industrial-scale electrochemical H₂O₂ production or for more practical uses such as paired electrolyzers that concurrently produce two valuable products or other industrial remediation that use H₂O₂ for mineralizing or electrochemically eliminating organic pollutants.

This work aims to streamline and create an economically viable electrochemical cell that can rival conventional methods by altering various components and redesigning expensive elements through cell engineering and catalyst design. This will enable future electrochemical processes to achieve a new level of sustainable chemical production.

Appendix A. Supplementary data

Equations, additional structural characterization and supporting electrochemical characterization.

Author Information

Corresponding Author

Wenzhen Li - Chemical and Biological Engineering, Biorenewables Research Laboratory, Iowa State University, Ames, IA 50011, USA. E-mail: wzli@iastate.edu; Tel: +1-515-294-4582

Authors

Basil Rawah - Chemical and Biological Engineering, Biorenewables Research Laboratory, Iowa State University, Ames, IA 50011, USA; Email: bsr23@iastate.edu

Mohammad Albloushi - Chemical and Biological Engineering, Biorenewables Research Laboratory, Iowa State University, Ames, IA 50011, USA; mbhador@iastate.edu

Acknowledgments

This research is partially supported by the USDA grant (20216702134650) and NSF CBET1947435. In particular, B.Rawah would like to thank Dapeng Jing for his help with SEM characterization and XPS, Michael Lee and Dr.Chris Cornelius for their assistance with contact angle measurements, Carolina Selvati for her help with XRD, and Dr.Yifu Chen, Tianlei Li, Xiaopeng Liu, and Sujin Kang for their insightful comments and suggestions. W. Li acknowledges

his Herbert L. Stiles Faculty Fellowship, and ISU Presidential Interdisciplinary Research Initiative (PIRI) grant. Open Access funding provided by the Iowa State University Library.

References

- [1] X. Sheng, B. Wouters, T. Breugelmans, A. Hubin, I.F. Vankelecom, P.P. Pescarmona, Cu/CuxO and Pt nanoparticles supported on multi-walled carbon nanotubes as electrocatalysts for the reduction of nitrobenzene, Appl. Catal. B . 147 (2014) 330-339. https://doi.org/10.1016/j.apcatb.2013.09.006.
- [2] J.M. Campos-Martin, G. Blanco-Brieva, J.L. Fierro, Hydrogen peroxide synthesis: an outlook beyond the anthraquinone process, Angew. Chem., Int. Ed. 45(42) (2006) 6962-6984. https://doi.org/10.1002/anie.200503779.
- [3] R. Arrigo, M.E. Schuster, S. Abate, G. Giorgianni, G. Centi, S. Perathoner, S. Wrabetz, V. Pfeifer, M. Antonietti, R. Schlögl, Pd supported on carbon nitride boosts the direct hydrogen peroxide synthesis, Acs Catal 6(10) (2016) 6959-6966. https://doi.org/10.1021/acscatal.6b01889.
- [4] B.S. Rawah, M. Albloushi, W. Li, Highly Efficient Electrochemical Synthesis of Hydrogen Peroxide (H2O2) Enabled by Amino Acid Glycine-Derived Metal-Free Nitrogen-Doped Ordered Mesoporous Carbon, ACS Sustain. Chem. Eng 10(17) (2022) 5453-5462. https://doi.org/10.1021/acssuschemeng.1c08285.
- [5] J.S. Jirkovský, I. Panas, E. Ahlberg, M. Halasa, S. Romani, D.J. Schiffrin, Single atom hotspots at Au–Pd nanoalloys for electrocatalytic H2O2 production, J. Am. Chem. Soc. 133(48) (2011) 19432-19441. https://doi.org/10.1021/ja206477z.
- [6] A. Verdaguer-Casadevall, D. Deiana, M. Karamad, S. Siahrostami, P. Malacrida, T.W. Hansen, J. Rossmeisl, I. Chorkendorff, I.E.L. Stephens, Trends in the electrochemical synthesis of H2O2: enhancing activity and selectivity by electrocatalytic site engineering, Nano Lett. 14(3) (2014) 1603-1608. https://doi.org/10.1021/nl500037x.
- [7] S. Siahrostami, A. Verdaguer-Casadevall, M. Karamad, D. Deiana, P. Malacrida, B. Wickman, M. Escudero-Escribano, E.A. Paoli, R. Frydendal, T.W. Hansen, I. Chorkendorff, I.E. Stephens, J. Rossmeisl, Enabling direct H2O2 production through rational electrocatalyst design, Nat Mater 12(12) (2013) 1137-43. https://doi.org/10.1038/nmat3795.
- [8] B.S. Rawah, W. Li, Electrocatalytic generation of hydrogen peroxide on cobalt nanoparticles embedded in nitrogen-doped carbon, Chinese J. Catal. 42(12) (2021) 2296-2305. https://doi.org/https://doi.org/10.1016/S1872-2067(21)63804-4.

- [9] X. Sheng, N. Daems, B. Geboes, M. Kurttepeli, S. Bals, T. Breugelmans, A. Hubin, I.F.J. Vankelecom, P.P. Pescarmona, N-doped ordered mesoporous carbons prepared by a two-step nanocasting strategy as highly active and selective electrocatalysts for the reduction of O2 to H2O2, Appl. Catal. B . 176 (2015) 212-224. https://doi.org/10.1016/j.apcatb.2015.03.049.
- [10] W. Li, A. Bonakdarpour, E. Gyenge, D.P. Wilkinson, Design of bifunctional electrodes for co-generation of electrical power and hydrogen peroxide, J. Appl. Electrochem. 48(9) (2018) 985-993. https://doi.org/10.1007/s10800-018-1232-0.
- [11] W. Li, A. Bonakdarpour, E. Gyenge, D.P. Wilkinson, Drinking Water Purification by Electrosynthesis of Hydrogen Peroxide in a Power-Producing PEM Fuel Cell, ChemSusChem 6(11) (2013) 2137-2143. https://doi.org/https://doi.org/10.1002/cssc.201300225.
- [12] I. Yamanaka, T. Murayama, Neutral H2O2 Synthesis by Electrolysis of Water and O2, Angew. Chem., Int. Ed. 47(10) (2008) 1900-1902. https://doi.org/https://doi.org/10.1002/anie.200704431.
- [13] C. Xia, Y. Xia, P. Zhu, L. Fan, H. Wang, Direct electrosynthesis of pure aqueous H2O2 solutions up to 20% by weight using a solid electrolyte, sci 366(6462) (2019) 226-231. https://doi.org/10.1126/science.aay1844.
- [14] Y. Sun, I. Sinev, W. Ju, A. Bergmann, S.r. Dresp, S. Kühl, C. Spöri, H. Schmies, H. Wang, D. Bernsmeier, Efficient electrochemical hydrogen peroxide production from molecular oxygen on nitrogen-doped mesoporous carbon catalysts, Acs Catal 8(4) (2018) 2844-2856. https://doi.org/10.1021/acscatal.7b03464.
- [15] Y. Sun, S. Li, Z.P. Jovanov, D. Bernsmeier, H. Wang, B. Paul, X. Wang, S. Kühl, P. Strasser, Structure, Activity, and Faradaic Efficiency of Nitrogen-Doped Porous Carbon Catalysts for Direct Electrochemical Hydrogen Peroxide Production, ChemSusChem 11(19) (2018) 3388-3395. https://doi.org/10.1002/cssc.201801583.
- [16] J. Park, Y. Nabae, T. Hayakawa, M.-a. Kakimoto, Highly selective two-electron oxygen reduction catalyzed by mesoporous nitrogen-doped carbon, Acs Catal 4(10) (2014) 3749-3754. https://doi.org/10.1021/cs5008206.
- [17] D. Sebastián, I. Suelves, R. Moliner, M.J. Lázaro, The effect of the functionalization of carbon nanofibers on their electronic conductivity, Carbon 48(15) (2010) 4421-4431. https://doi.org/https://doi.org/10.1016/j.carbon.2010.07.059.
- [18] Y. Xu, K. Sheng, C. Li, G. Shi, Highly conductive chemically converted graphene prepared from mildly oxidized graphene oxide, J. Mater. Chem. 21(20) (2011) 7376-7380. https://doi.org/10.1039/C1JM10768B.
- [19] N. Morimoto, T. Kubo, Y. Nishina, Tailoring the Oxygen Content of Graphite and Reduced Graphene Oxide for Specific Applications, Sci. Rep. 6(1) (2016) 21715. https://doi.org/10.1038/srep21715.

- [20] N. Ul Hassan, M. Mandal, G. Huang, H.A. Firouzjaie, P.A. Kohl, W.E. Mustain, Achieving High-Performance and 2000 h Stability in Anion Exchange Membrane Fuel Cells by Manipulating Ionomer Properties and Electrode Optimization, Advanced Energy Materials 10(40) (2020) 2001986. https://doi.org/https://doi.org/10.1002/aenm.202001986.
- [21] J.R. Varcoe, P. Atanassov, D.R. Dekel, A.M. Herring, M.A. Hickner, P.A. Kohl, A.R. Kucernak, W.E. Mustain, K. Nijmeijer, K. Scott, T. Xu, L. Zhuang, Anion-exchange membranes in electrochemical energy systems, Energy Environ. Sci. 7(10) (2014) 3135-3191. https://doi.org/10.1039/C4EE01303D.
- [22] D.R. Dekel, Review of cell performance in anion exchange membrane fuel cells, J. Power Sources 375 (2018) 158-169. https://doi.org/https://doi.org/10.1016/j.jpowsour.2017.07.117.
- [23] N.V. Klassen, D. Marchington, H.C.E. McGowan, H2O2 determination by the I3-method and by KMnO4 titration, Anal. Chem. 66(18) (1994) 2921-2925. https://doi.org/10.1021/ac00090a020.
- [24] M. Kozlowski, A. Kozlowska, Comparison of electrically conductive fillers in polymer systems, Macromol. Symp. 108(1) (1996) 261-268. https://doi.org/https://doi.org/10.1002/masy.19961080121.
- [25] X. Yang, K. Li, D. Cheng, W.-L. Pang, J. Lv, X. Chen, H.-Y. Zang, X.-L. Wu, H.-Q. Tan, Y.-H. Wang, Nitrogen-doped porous carbon: Highly efficient trifunctional electrocatalyst for oxygen reversible catalysis and nitrogen reduction reaction, J. Mater. Chem. A 6(17) (2018) 7762-7769. https://doi.org/10.1039/c8ta01078a.
- [26] I.-A. Choi, D.-H. Kwak, S.-B. Han, J.-Y. Park, H.-S. Park, K.-B. Ma, D.-H. Kim, J.-E. Won, K.-W. Park, Doped porous carbon nanostructures as non-precious metal catalysts prepared by amino acid glycine for oxygen reduction reaction, Appl. Catal. B . 211 (2017) 235-244. https://doi.org/10.1016/j.apcatb.2017.04.039.
- [27] C. Xia, J.Y. Kim, H. Wang, Recommended practice to report selectivity in electrochemical synthesis of H2O2, Nat. Catal 3(8) (2020) 605-607. https://doi.org/10.1038/s41929-020-0486-1.
- [28] Y. Qiu, J. Huo, F. Jia, B.H. Shanks, W. Li, N-and S-doped mesoporous carbon as metal-free cathode catalysts for direct biorenewable alcohol fuel cells, J. Mater. Chem. A 4(1) (2016) 83-95. https://doi.org/10.1039/c5ta06039g.
- [29] L. Li, C. Tang, Y. Zheng, B. Xia, X. Zhou, H. Xu, S.Z. Qiao, Tailoring selectivity of electrochemical hydrogen peroxide generation by tunable pyrrolic-nitrogen-carbon, Advanced Energy Materials 10(21) (2020) 2000789. https://doi.org/10.1002/aenm.202000789.
- [30] Y. Ding, W. Zhou, J. Gao, F. Sun, G. Zhao, H2O2 Electrogeneration from O2 Electroreduction by N-Doped Carbon Materials: A Mini-Review on Preparation Methods, Selectivity of N Sites, and Prospects, Adv. Mater. Interfaces 8(10) (2021) 2002091. https://doi.org/doi.org/10.1002/admi.202002091.

- [31] X. Bao, X. Nie, D. von Deak, E.J. Biddinger, W. Luo, A. Asthagiri, U.S. Ozkan, C.M. Hadad, A first-principles study of the role of quaternary-N doping on the oxygen reduction reaction activity and selectivity of graphene edge sites, Top Catal 56(18) (2013) 1623-1633. https://doi.org/10.1007/s11244-013-0097-z.
- [32] X. Lu, D. Wang, L. Ge, L. Xiao, H. Zhang, L. Liu, J. Zhang, M. An, P. Yang, Enriched graphitic N in nitrogen-doped graphene as a superior metal-free electrocatalyst for the oxygen reduction reaction, NJC 42(24) (2018) 19665-19670. https://doi.org/10.1039/c8nj04857f.
- [33] H.W. Kim, M.B. Ross, N. Kornienko, L. Zhang, J. Guo, P. Yang, B.D. McCloskey, Efficient hydrogen peroxide generation using reduced graphene oxide-based oxygen reduction electrocatalysts, Nat. Catal 1(4) (2018) 282-290. https://doi.org/10.1038/s41929-018-0044-2.
- [34] Y. Sun, L. Silvioli, N.R. Sahraie, W. Ju, J. Li, A. Zitolo, S. Li, A. Bagger, L. Arnarson, X. Wang, T. Moeller, D. Bernsmeier, J. Rossmeisl, F. Jaouen, P. Strasser, Activity—Selectivity Trends in the Electrochemical Production of Hydrogen Peroxide over Single-Site Metal—Nitrogen—Carbon Catalysts, J. Am. Chem. Soc. 141(31) (2019) 12372-12381. https://doi.org/10.1021/jacs.9b05576.
- [35] N. Ramaswamy, S. Mukerjee, Influence of Inner- and Outer-Sphere Electron Transfer Mechanisms during Electrocatalysis of Oxygen Reduction in Alkaline Media, J. Phys. Chem. C . 115(36) (2011) 18015-18026. https://doi.org/10.1021/jp204680p.
- [36] D. Pletcher, R.A. Green, R.C.D. Brown, Flow electrolysis cells for the synthetic organic chemistry laboratory, Chem. Rev. 118(9) (2017) 4573-4591. https://doi.org/10.1021/acs.chemrev.7b00360.
- [37] D. Fang, H. Zhang, L. He, J. Geng, W. Song, S. Sun, Z. Shao, B. Yi, Facile Synthesis of Nanoporous Pt-Encapsulated Ir Black as a Bifunctional Oxygen Catalyst via Modified Polyol Process at Room Temperature, ChemElectroChem 6(14) (2019) 3633-3643. https://doi.org/https://doi.org/10.1002/celc.201900824.
- [38] D. Fang, X. Tang, L. Yang, D. Xu, H. Zhang, S. Sun, Z. Shao, B. Yi, Facile synthesis of Ptdecorated Ir black as a bifunctional oxygen catalyst for oxygen reduction and evolution reactions, Nanoscale 11(18) (2019) 9091-9102. https://doi.org/10.1039/C9NR00279K.
- [39] W.R.P. Barros, R.M. Reis, R.S. Rocha, M.R.V. Lanza, Electrogeneration of hydrogen peroxide in acidic medium using gas diffusion electrodes modified with cobalt (II) phthalocyanine, Electrochim. Acta 104 (2013) 12-18. https://doi.org/https://doi.org/10.1016/j.electacta.2013.04.079.
- [40] M. Jahan, Z. Liu, K.P. Loh, A Graphene Oxide and Copper-Centered Metal Organic Framework Composite as a Tri-Functional Catalyst for HER, OER, and ORR, Adv. Funct. Mater. 23(43) (2013) 5363-5372. https://doi.org/https://doi.org/10.1002/adfm.201300510.
- [41] Z. Chen, S. Chen, S. Siahrostami, P. Chakthranont, C. Hahn, D. Nordlund, S. Dimosthenis, J.K. Nørskov, Z. Bao, T.F. Jaramillo, Development of a reactor with carbon catalysts for

modular-scale, low-cost electrochemical generation of H2O2, React. Chem. Eng. 2(2) (2017) 239-245. https://doi.org/10.1039/C6RE00195E.